Buffered-cluster method for hybridization of density-functional theory and classical molecular dynamics: Application to stress-dependent reaction of H_2O on nanostructured Si

Shuji Ogata

Graduate School of Engineering, Nagoya Institute of Technology, Gokiso-Cho, Showa-ku, Nagoya 466-8555, Japan

(Received 18 March 2005; revised manuscript received 31 May 2005; published 21 July 2005)

A hybrid density-functional-theory and molecular-dynamics simulation scheme was proposed [Ogata *et al.*, Comput. Phys. Commun. **149**, 30 (2002)] in which a total atomistic system is partitioned, in real space, into the quantum (QM) region whose electronic structure is calculated with the density-functional theory and the classical (CL) region treated with the interatomic potential for the molecular dynamics. In the scheme, the link-atom method that uses hydrogen atoms for termination of the QM atoms is adopted to couple the QM and CL regions mechanically. A proper choice of the QM region that retains the original atomic configuration is limited in the link-atom method. In this paper we propose a coupling method, called the buffered-cluster method, with the introduction of buffer atoms to minimize possible effects arising from the finiteness of the size of the QM region. The buffered-cluster method is applicable to any reasonable choice of the QM region in a wide range of ceramics and semiconductor materials. The accuracy of the buffered-cluster method is analyzed by applying it to crystalline Si and alumina systems, to find little differences around the QM-CL boundaries in both relaxed configuration of the atoms and recoil forces on them due to their trial displacements. The insensitivity of the atomic forces to the choice of the QM region in the buffered-cluster method makes it possible to rechoose the QM region adaptively during the hybrid simulation run for fast computation. The hybrid simulation scheme with the buffered-cluster method is applied to analyze adsorption and dissociation processes of an H_2O molecule on a notched Si-slab system with or without strains, in which the H_2O interacts with the notch-bottom facet of Si(100)-(2×1) dimer structure. The QM region is chosen in the system to cover the reaction region. Energy variations along the reaction paths show that the adsorption energy and the dissociation barrier of the H_2O molecule on the Si(100) facet in the system are sensitive to the stain. The adsorption energy decreases substantially, while the dissociation barrier with H transferred to a nearby dimer increases, when the system is stretched. We perform hybrid simulation runs with the buffered-cluster method to study the adsorption and dissociation dynamics of the H_2O molecule with the facet of Si(100)-(2×1) in the nanostructured Si system at both stretched and unstrained conditions, in which the QM region is rechosen dynamically to trace the reaction atoms. The probability of the H_2O dissociation and the following H-transfer path depend significantly on the strain applied to the system and on the initial conditions of the molecule.

DOI: 10.1103/PhysRevB.72.045348 PACS number(s): 68.35.Md, 73.22.−f, 82.20.Wt, 31.15.Qg

I. INTRODUCTION

Microscopic instruments such as the atomic force microscope[1] and the microelectromechanical system[2] (MEMS) have advanced greatly in recent years. They have enabled us to investigate various quantities of materials including friction, fatigue, and failure at nanometer scales.[1,2] Failures of the standard scaling relations have often been observed for the quantities. The stick-slip process[3] occurs in the friction between the nanosystems. The Hall-Petch law[4] for the material strength based on the continuum mechanics fails for nanophase materials.[5,6] Computer-aided modeling is therefore expected to play important roles to reduce costs and times in both designing a variety of the nanosystems[7,8] and predicting their lifetimes.

One of the principal characteristics of the nanosystem is concurrent coupling of the multiscale processes in it. For instance, when we consider dynamical failure of the nanosystem under stress, internal stress related to its shape and size will affect the electronic structure and hence the chemical reactivity in the nanosystem; on the other hand, produced heat due to the chemical reactions will promote dynamic deformation of the nanosystem. An efficient approach to treat the multiscale processes theoretically is to hybridize proper simulation methods.[9] In the hybrid approach, a simulation system is partitioned in real space into multiscale regions. A hierarchical set of theoretical calculation methods—for instance, the electronic structure calculation, the classical atomistic method, and the continuum method—is then applied appropriately to the regions.[10]

Many of the interesting processes in materials involve chemical reactions between constituent atoms. Classical (CL) atomistic methods such as the molecular-dynamics (MD) method using an empirical interatomic potential fail often to describe such processes. Interatomic interaction in the reaction region should be calculated with a quantum-mechanical (QM) method that can describe breaking and formation of the atomic bonds. Heat produced in the reaction region should be transferred correctly to the surrounding region. Therefore it is required to treat large-scale atomistic systems with quantum accuracies. There have been growing interests[10] in developing hybrid QM-CL simulation schemes, in which a reaction region treated by a QM method is embedded in a classical system of atoms interacting via an empirical interatomic potential.

 ©2005 The American Physical Society

During the past decade, computationally efficient QM approaches based on density-functional theory[11–13] (DFT) have advanced greatly. A hybrid QM-CL simulation scheme[14] employing DFT for the QM calculation and the molecular mechanics for the CL calculation was therewith proposed for simulation of biological molecules. In the scheme, plane waves are used as the basis to solve the Kohn-Sham equations for valence electrons in the QM region. Independently, Ogata *et al.*[15,16] developed a similar hybrid QM-CL scheme for materials simulation by employing real-space DFT in which both wave functions and pseudopotentials are represented on uniform Cartesian mesh points in real space.[17] The DFT code[18] is parallelized based on the spatial decomposition, and a few hundred atoms can be treated on thousands of processors. Both hybrid schemes employ the link-atom method to couple the QM and CL regions, and use H atoms for termination of the chemical bonds broken artificially at the QM-CL boundary. Different formulas are used to determine position of the termination-H atom as a function of that of the QM and CL atoms in the broken bond. Ogata *et al.*[19,20] successfully applied the hybrid QM-CL simulation scheme to Si systems with environmental H_2O molecules to study moisture effects on fracture initiation in Si. A partially cracked Si system under tension (mode-I opening) with crack walls of Si(110) was simulated with multiple H_2O molecules put around the crack front. Electronic structures near the crack front are calculated with DFT. The DFT description is embedded in the system of classical atoms interacting through an empirical potential. The simulation results[19,20] showed that the reaction of H_2O molecules at the crack tip of Si is sensitive to the stress intensity factor.[4] Such a successful simulation required a careful choice of the QM region. An inappropriate choice of the QM region resulted in an unwanted deformation of the atomic configuration near the QM-CL boundary.

Such sensitivity of simulation results to the choice of QM region prevents the hybrid simulation scheme from being applied to various engineering problems. Motivated by this, we will introduce in this paper a coupling method between the QM and CL regions without using the link atoms and will demonstrate that the method is applicable to any reasonable choice of the QM region in both Si and alumina systems with accurate mechanical coupling between the QM and CL regions. The insensitivity of our coupling method to changing the QM region makes it possible to rechoose the QM region dynamically in an adaptive way during the simulation run.

Reaction of H_2O with Si surface is one of the fundamental processes in producing computer chips to create thin insulator (SiO_2) films. Understanding the stress dependence of the H_2O reaction with Si is also essential in designing mechanical components of MEMS,[21] which are usually made of Si and supposed to be used in corrosive environments such as inside of human body. We will apply the hybrid simulation scheme with our coupling method to absorption and dissociation processes of an H_2O molecule on a nanostructured Si system under stress. Those atoms around the H_2O will be treated with the DFT, while the surroundings with the MD method. We will show that the adsorption energy and dissociation barriers of the H_2O molecule on the Si(100) facet of the system are sensitive to the degree of the stress. The adsorption energy decreases substantially, while the dissociation barrier with H transferred to a nearby dimer increases, when the system is stretched. Hybrid simulation runs with our coupling method will be performed at both stretched and unstrained conditions to study the reaction dynamics of the H_2O molecule with the buckling Si-Si dimers on the Si(100) facet in the nanostructured Si system, in which the QM region is rechosen dynamically to trace the reaction atoms. Dissociation of the H_2O molecule and the H-transfer path depend significantly on the strain applied to the system and on the initial conditions of the molecule. We will demonstrate that the H atom dissociated from the H_2O molecule has substantial probabilities to adsorb to a neighboring dimer in the unstrained Si systems and that the H atom adsorbs with high probabilities to the same dimer in the stretched systems.

In Sec. II, we will first explain the link-atom method in the hybrid QM-CL simulation scheme and its limitation in an appropriate choice of the QM region. Then we will introduce a coupling method that overcomes the limitation. Various analyses will be performed to demonstrate the proper mechanical couplings of the QM and CL regions in Si and alumina systems. The hybrid simulation scheme with our coupling method will be applied to reaction of an H_2O molecule with nanostructured Si in Sec. III. Concluding remarks will be given in Sec. IV.

II. IMPROVEMENT IN THE COUPLING METHOD

Let us consider a model system of crystalline Si to compare our former and present coupling methods in the hybrid simulation scheme. The system contains mutually nonoverlapping regions of reasonable sizes to be treated with a QM method; atoms in those QM regions are called the QM atoms. The rest of the QM atoms are the CL atoms. To make formulation explicitly, we assume the empirical, classical interatomic potential by Stillinger and Weber[22] (SW) for the CL calculation of Si. We choose the DFT as the QM method by considering balance between the accuracy and computation speed, though any calculation method that predicts the electronic structures of the atomic clusters such as the tight-binding method[23] may be used. In Sec. II A, we will summarize our former coupling method that connects the QM and CL regions dynamically using the link atoms. Our current coupling method will be introduced in Sec. II B with various tests of its accuracy and stability.

A. Link-atom method

To describe the total energy of the hybridized system, Ogata *et al.*[15,16] followed the modular approach by Svensson *et al.*[24] and Eichler *et al.*[25] and wrote it in a linear combination form. The Hamiltonian that predicts dynamics of all the atoms is

$$H(R_{\rm all},P_{\rm all}) = H_{\rm CL}^{\rm system}(R_{\rm all},P_{\rm all}) + \sum_{\rm cluster} (E_{\rm QM}^{\rm cluster} - E_{\rm CL}^{\rm cluster}), \tag{1}$$

where $R_{\rm all}$ and $P_{\rm all}$ represent sets of positions and momenta of all the atoms, respectively. The $H_{\rm CL}^{\rm system}$ in Eq. (1) is the

classical Hamiltonian for the total system composed of the kinetic energy and the potential energy terms: $H_{\mathrm{CL}}^{\mathrm{system}} = E_{\mathrm{kin}}(P_{\mathrm{all}}) + E_{\mathrm{CL}}^{\mathrm{system}}(R_{\mathrm{all}})$. The last two terms on the right-hand side of Eq. (1) may be understood as a quantum correction to the classical potential energy for the QM region.

We denote sets of positions of the CL and the QM atoms as $\{r_{\mathrm{CL}}\}$ and $\{r_{\mathrm{QM}}\}$, respectively—that is, $R_{\mathrm{all}} = \{r_{\mathrm{CL}}\} + \{r_{\mathrm{QM}}\}$. The CL atoms contain the handshake[15,16] (HS) atoms, which are those atoms adjacent to the surface atoms of the QM region in the total system; the positions of the HS atoms are $\{r_{\mathrm{QM\text{-}CL}}^{\mathrm{HS}}\}$. In the link-atom method, the last two terms on the right-hand side of Eq. (1) are functions of $\{r_{\mathrm{QM}}\}$ and $\{r_{\mathrm{QM\text{-}CL}}^{\mathrm{HS}}\}$:

$$E_{\mathrm{QM}}^{\mathrm{cluster}} = E_{\mathrm{QM}}^{\mathrm{cluster}}(\{r_{\mathrm{QM}}\};\{r_{\mathrm{QM\text{-}CL}}^{\mathrm{HS}}\}), \quad (2)$$

$$E_{\mathrm{CL}}^{\mathrm{cluster}} = E_{\mathrm{CL}}^{\mathrm{cluster}}(\{r_{\mathrm{QM}}\};\{r_{\mathrm{QM\text{-}CL}}^{\mathrm{HS}}\}). \quad (3)$$

For both QM and CL calculations for the QM region in Eqs. (2) and (3), termination atoms are introduced at the dangling-bond sites of the QM atoms corresponding to the broken bonds at the QM-CL boundaries. The termination atoms are hydrogen for the QM calculation, while they are silicon for the CL calculation. The position of the termination-H atom is determined from that of the corresponding HS atom and its bonding-pair QM atom as follows. Let $r_{\mathrm{QM}}(j;i)$ be the positions of the QM atoms $(j=1,2,\ldots)$ bonding to the target HS atom i at $r_{\mathrm{QM\text{-}CL}}^{\mathrm{HS}}(i)$; depending on choice of QM region, a plural number of different j may exist for the HS atom i. The termination-H atom is placed at $r^{\mathrm{H}} = \beta r_{\mathrm{QM\text{-}CL}}^{\mathrm{HS}}(i) + (1-\beta) r_{\mathrm{QM}}(j;i)$ for each (i,j) pair with scaling factor $\beta = 0.66$. The value of β is determined by comparing the relaxed configuration of the free $\mathrm{SiH_4}$ cluster and the crystalline configuration of Si with the diamond structure. For the CL calculation of the QM region, termination-Si atoms are set at the same positions of the HS atoms—i.e., $r^{\mathrm{Si}} = r_{\mathrm{QM\text{-}CL}}^{\mathrm{HS}}(i)$. If the CL interatomic potential is a two-body one, the HS atom at $r_{\mathrm{QM\text{-}CL}}^{\mathrm{HS}}(i)$ interacts with the QM atom at $r_{\mathrm{QM}}(j;i)$ through the QM energy $E_{\mathrm{QM}}^{\mathrm{cluster}}$.

Figure 1 shows a schematic view of the atomic configuration around the QM-CL boundary in the link-atom method. In Fig. 1, the white spheres denote the CL atoms, while the black spheres the QM atoms. The termination-H atoms are set on the broken Si-Si bonds at the QM-CL boundaries. Dotted lines are drawn between the termination-H atoms and the relating HS atoms for the guide to the eyes. We note that if a single HS atom corresponds to a plural number of termination-H atoms, the termination-H atoms get close to each other; the minimum interparticle distance is only 1.78 Å in the case of Si crystal with the diamond structure. Displacement of the HS atom—i.e., one of the CL atoms—creates that of the relating termination-H atoms. And the displacements of the termination-H atoms change the forces on the QM atoms, which are calculated with the QM method. Hence, at the QM-CL boundary, the HS atom interacts with the QM atom through the QM force on the termination-H atoms.

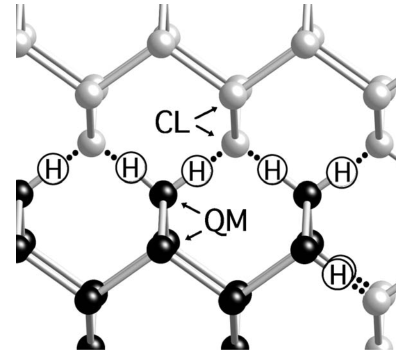

FIG. 1. Close-up view of the QM-CL boundary in the hybrid QM-CL simulation of crystalline Si with the link-atom method. The black spheres correspond to the QM-Si atoms, while the white spheres to the CL-Si atoms. The termination-H atoms introduced for the QM calculation of the QM region with the link-atom method are drawn to guide the eye.

The link-atom method has been the standard to couple the QM region with the CL region in the hybrid simulation scheme for biochemical molecules. For the scaling factor β which is used to determine the position of the termination H, $r^{\mathrm{H}} = \beta r_{\mathrm{QM\text{-}CL}}^{\mathrm{HS}} + (1-\beta) r_{\mathrm{QM}}$, in the QM calculation, Eichner *et al.*[25] set $\beta(a) = \beta_{-1}/a$ with $a = |r_{\mathrm{QM\text{-}CL}}^{\mathrm{HS}} - r_{\mathrm{QM}}|$ in order to fix $|r^{\mathrm{H}} - r_{\mathrm{QM}}| = \beta_{-1}$. Dapprich *et al.*[26] set a constant value to β: $\beta(a) = \beta_0$. Eichinger *et al.*[14] proposed to take $\beta(a) = \beta_{-1}/a + \beta_0$ for improved mechanical coupling between the QM and the HS atoms. Ogata *et al.*[15,16] assumed $\beta(a) = \beta_0$ and then generalized it to[27] $\beta(a) = \beta_0 + \beta_1 a$, demonstrating similar accuracy with that in Eichinger *et al.*[14]

By calculating the gradient of H in Eq. (1) analytically with respect to the position r_i of atom i, we obtain the force F_i on the atom as $F_i = -\partial H/\partial r(i) = F_{\mathrm{CL},i}^{\mathrm{system}} + \sum_{\mathrm{cluster}}(F_{\mathrm{QM},i}^{\mathrm{cluster}} - F_{\mathrm{CL},i}^{\mathrm{cluster}})$ with $F_{\mathrm{CL},i}^{\mathrm{system}} = -\partial E_{\mathrm{CL}}^{\mathrm{system}}/\partial r_i$, $F_{\mathrm{QM},i}^{\mathrm{cluster}} = -\partial E_{\mathrm{QM}}^{\mathrm{cluster}}/\partial r_i$, and $F_{\mathrm{CL},i}^{\mathrm{cluster}} = -\partial E_{\mathrm{CL}}^{\mathrm{cluster}}/\partial r_i$. Note that $F_{\mathrm{CL},i}^{\mathrm{system}}$ and $F_{\mathrm{CL},i}^{\mathrm{cluster}}$ cancel each other for the QM atoms. Since $\partial E_{\mathrm{QM}}^{\mathrm{cluster}}/\partial r_{\mathrm{QM\text{-}CL}}^{\mathrm{HS}} = (\partial E_{\mathrm{QM}}^{\mathrm{cluster}}/\partial r^{\mathrm{H}})(dr^{\mathrm{H}}/dr_{\mathrm{QM\text{-}CL}}^{\mathrm{HS}})$ and $\partial E_{\mathrm{QM}}^{\mathrm{cluster}}/\partial r_{\mathrm{QM}} = (\partial E_{\mathrm{QM}}^{\mathrm{cluster}}/\partial r_{\mathrm{QM}})_{r^{\mathrm{H}}\mathrm{fixed}} + (\partial E_{\mathrm{QM}}^{\mathrm{cluster}}/\partial r^{\mathrm{H}}) \times (dr^{\mathrm{H}}/dr_{\mathrm{QM}})$, the force on the termination H obtained in the QM calculation contributes to both HS and QM atoms.

The electronic structure of the QM region is evaluated with the DFT. Details of the DFT code have been explained in Refs. 15, 16, and 18. The Kohn-Sham (KS) formulation is adopted to calculate the total energy $E_{\mathrm{QM}}^{\mathrm{cluster}}$ of the atomic cluster. Only valence electrons are considered with the norm-conserving pseudopotentials. The generalized gradient approximation[28] to the exchange correlation potential of the electrons is adopted with the partial-core correction. Cartesian mesh points in real space are used to represent the KS orbitals and Hartree potential. Derivatives of the orbitals are evaluated with the sixth-order finite-difference method.[17] Data on the mesh points are spatially decomposed and stored in compute nodes for fast computation on a parallel computer. Numerical solutions of the KS orbitals and of the Hartree field are obtained on the mesh points with the multigrid method[29] for accelerated convergence in the self-consistency-field iterations. Atoms with species H, Si, and O

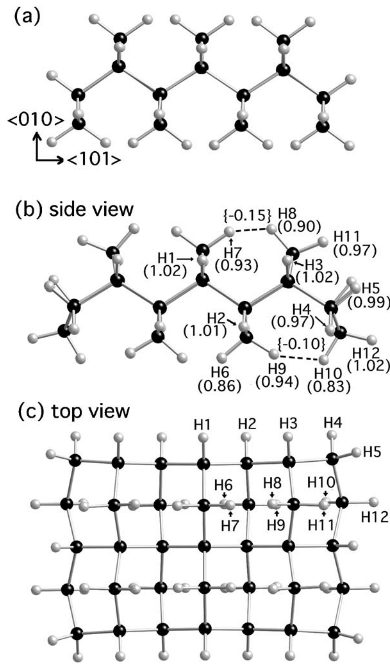

FIG. 2. (a) An example of the atomic cluster for the QM calculation in the hybrid QM-CL simulation of crystalline Si with the link-atom method; the black spheres correspond to the QM-Si atoms, while the white spheres to the termination-H atoms. (b) Side view of the minimum-energy configuration of the atomic cluster obtained with the DFT (i.e., QM) method under the free-boundary condition starting from the configuration shown in (a). The numbers in { } denote the Mulliken's overlap populations for the Si-Si bonds, those in ( ) the Mulliken's populations for the atoms. (c) Same as (b) but for the top view.

will be involved in the hybrid simulation in Sec. III. Finer mesh points are used for the KS orbitals in the vicinity of the O atom following the double-grid method.[30] Fourier components of the local and nonlocal pseudopotentials with wavelengths shorter than the mesh size are suppressed using the King-Smith method.[13] The mesh size for Si is $h=0.55$ a.u., which corresponds to a cutoff energy of $(\pi/h)^2 \sim 33$ Ry in the plane-wave representation of the KS orbitals.

One of the most significant problems of the link-atom method, which hinders its usage in a wide range of the engineering problems, is that the most stable atomic configuration is fairly sensitive to choice of the QM region in the total system. In the former hybrid simulations of the nanostructured Si systems, the QM regions were chosen carefully after various stability tests. If we choose an inappropriate set of the QM atoms in crystalline Si, the atomic configuration near the QM-CL boundary distorts significantly as the total energy H is minimized. To understand the reasons for it, we consider an example of the atomic cluster to be used for the QM calculation in the hybrid simulation of crystalline Si shown in Fig. 2(a); the black spheres denote Si atoms and the white spheres H atoms for termination. Note that H atoms at the top and the bottom in Fig. 2(a) are sitting in close proximity to each other. By relaxing all the atoms of the cluster in Fig. 2(a) to find the ground state of it under the free-boundary condition, we find significant distortion of the atomic configuration as shown in Figs. 2(b) and 2(c). Also shown in Figs. 2(b) and 2(c) are the Mulliken's atomic populations[31,32] and overlap populations[31,32] of the valence electrons. We thereby find that those proximate H atoms charge more positively—i.e., smaller atomic population—as compared to other H atoms and that the overlap populations between the proximate H atoms become negative, indicating antibonding character. The facts demonstrate that the proximate H atoms have a tendency to repel each other. Since positions of the termination-H atoms relate directly to that of the CL atoms in the link-atom method, such repulsion deforms the crystalline structure significantly at the QM-CL boundary. If the QM-CL boundary corresponds to Si{111}, the termination H atoms are well separated from each other and therefore the link-atom method can be used.

We may consider that both QM and CL methods give zero forces to all the atoms in crystalline Si if all the atoms are treated with the same method. Usually the hybridized system treated with Eq. (1) has nonzero forces, called the ghost forces,[33] on those atoms located at the QM-CL boundaries as we have stated above, reflecting degree of inaccuracy in the coupling method. The ghost forces produce unwanted deformations in the Si system. We can easily think of two ways, at least, to remedy this. We can cancel such a ghost force by adding a fictitious force[33] to keep the crystalline structure of Si. Suppose we apply such a force-cancellation method to the hybrid simulation of a fracturing Si system, in which the QM region that includes bond-breaking sites evolves its size, shape, and position. In the simulation, we must prepare a table of the ghost forces by performing separate calculations at every time we rechoose the QM region. Since the overhead of such preparation calculations is substantial, the force-cancellation method is not quite useful. Alternatively, considering that the termination-H atoms should be well separated for a proper coupling, we can choose the QM region so that all facets of the region assume Si{111}. However, such a QM region will be generally much larger in size than expected, resulting in slow simulation. For the hybrid QM-CL simulation to have reasonable accuracy and computation speed, there should exist no such a restriction in the choice of the QM region.

Another problem in the link-atom method is that it is applicable to the materials of limited atomic species with well-defined chemical bonds. For example, when we have tried to apply the link-atom method to the hybridized α-Al_2O_3 crystal and set H atoms on the broken Al-O segments at the QM-CL boundaries, we have found that some of the H atoms have detached to form H_2 molecules. We have tried also to use "virtual atoms" with nonintegral numbers of core charge. However, we could not find proper atoms for termination purposes in the case of the α-Al_2O_3 system.

In Sec. II B we will introduce the buffered-cluster method, which is applicable to any reasonable choice of QM region in a variety of ceramic materials and requires little overhead when the QM region is rechosen during the simulation run.

B. Buffered-cluster method

We propose the buffered-cluster method for coupling of the QM and CL regions in the hybrid simulation scheme,

which requires no HS atoms and therefore no proximate termination-H atoms in the QM calculation of the QM region. Details of the buffered-cluster method are explained with its application mainly to crystalline Si, and various kinds of analyses are performed to confirm accuracy, stability, and portability of the method. Any reasonable choice of QM region is acceptable in the hybrid simulation of crystalline Si with the buffered-cluster method. The algorithm to rechoose the QM region adaptively during the hybrid simulation run is presented also for Si systems.

We consider a Si system with its atomic configuration around the QM-CL boundary assuming the diamond structure. In the buffered-cluster method, the cluster-energy terms on the right-hand side of Eq. (1) are functions of positions of the QM atoms $\{r_{\mathrm{QM}}\}$ only:

$$E_{\mathrm{QM}}^{\mathrm{cluster}} = E_{\mathrm{QM}}^{\mathrm{cluster}}(\{r_{\mathrm{QM}}\}), \tag{4}$$

$$E_{\mathrm{CL}}^{\mathrm{cluster}} = E_{\mathrm{CL}}^{\mathrm{cluster}}(\{r_{\mathrm{QM}}\}). \tag{5}$$

In both QM and CL calculations of the QM region in Eqs. (4) and (5), additional atoms are placed at the dangling-bond sites of the QM atoms at the QM-CL boundaries to buffer possible effects of the cutting bonds. We call those atoms as the buffer atoms.

For the CL calculation of the QM region in Eq. (5), the buffer atoms are Si to mimic the original bonds at the QM-CL boundary. Starting from positions of either the corresponding CL-Si atoms or the buffer-Si atoms at the last step, positions of the buffer-Si atoms are adjusted at every time step in the simulation run to minimize the potential energy $E_{\mathrm{CL}}^{\mathrm{cluster}}$ under the constraint of fixing $\{r_{\mathrm{QM}}\}$. Here, the buffer-Si atoms interact only with the bonding-pair Si atoms in the original system through the two- and the three-body terms of the SW interatomic potential. An example of the QM region in crystalline Si is shown in Fig. 3(a), in which the black spheres denote the QM atoms and the white spheres the CL atoms. Relating to the QM region chosen in Fig. 3(a), the atomic cluster for the CL calculation contains the buffer-Si atoms as depicted in Fig. 3(c). Note that the positions of the buffer atoms in the buffered-cluster method may differ from that of the corresponding CL atoms in the total system, while the positions of the termination-Si atoms in the link-atom method are the same as those of the HS atoms as has been explained in Sec. II A.

For the QM calculation of the QM region in Eq. (4), the buffer atoms are either H or Si depending on the bonding characteristics in the original system, as shown in Fig. 3(b): the small spheres in grey denote the buffer-H atoms and the large spheres in grey the buffer-Si atoms. The positions of the buffer atoms (either H or Si) for the QM calculation are determined by referring to those of the buffer atoms in the atomic cluster for the CL calculation in Fig. 3(c). If a buffer-Si atom located at $r_{\mathrm{CL}}^{\mathrm{buffer}}$ connects to a single QM atom at r_{QM} in the atomic cluster for the CL calculation, we put a buffer-H atom at $r_{\mathrm{b}}=\beta r_{\mathrm{CL}}^{\mathrm{buffer}}+(1-\beta)r_{\mathrm{QM}}$ with the scaling factor $\beta=0.66$ in the atomic cluster for the QM calculation. Otherwise, we put a buffer-Si atom at $r_{\mathrm{b}}=r_{\mathrm{CL}}^{\mathrm{buffer}}$ in the atomic cluster for the QM calculation. We note that positions of the buffer atoms are not relaxed in the atomic cluster for the QM calculation.

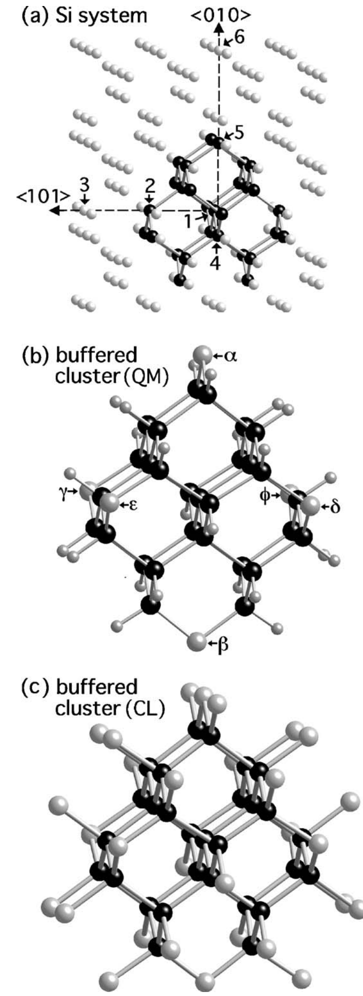

FIG. 3. (a) The QM atoms (black spheres) chosen in the hybrid QM-CL simulation of crystalline Si with the buffered-cluster method. Atoms 1, 2, and 3 are equivalent in the crystalline symmetry; likewise, atoms 4, 5, and 6 are equivalent. (b) The atomic cluster for the QM calculation of the QM region depicted in (a) with the buffered-cluster method. The large spheres in gray labeled with the Greek letters correspond to the buffer-Si atoms, while the small spheres in gray to the buffer-H atoms. (c) The atomic cluster for the CL calculation of the QM region depicted in (a) with the buffered-cluster method. The white spheres denote the buffer-Si atoms.

Since both $E_{\mathrm{QM}}^{\mathrm{cluster}}$ and $E_{\mathrm{CL}}^{\mathrm{cluster}}$ in Eqs. (4) and (5) are independent of the positions of the CL atoms $\{r_{\mathrm{CL}}\}$, the QM atoms interact with the CL atoms through the classical interatomic potential in $H_{\mathrm{CL}}^{\mathrm{system}}$. Explicit formulas of the atomic forces in the buffered-cluster method are the following. For QM atom i, the force

$$F_i = -\frac{\partial H}{\partial r_{\mathrm{QM},i}} = -\frac{\partial E_{\mathrm{CL}}^{\mathrm{system}}}{\partial r_{\mathrm{QM},i}} - \sum_{\mathrm{cluster}} \left(\frac{\partial E_{\mathrm{QM}}^{\mathrm{cluster}}}{\partial r_{\mathrm{QM},i}} - \frac{\partial E_{\mathrm{CL}}^{\mathrm{cluster}}}{\partial r_{\mathrm{QM},i}} \right), \tag{6}$$

with

$$\frac{\partial E_{\mathrm{QM}}^{\mathrm{cluster}}}{\partial r_{\mathrm{QM},i}} = \left(\frac{\partial E_{\mathrm{QM}}^{\mathrm{cluster}}}{\partial r_{\mathrm{QM},i}}\right)_{\mathrm{fix}\ \{r_b\}} + \sum_{j}^{\mathrm{buffer}} \frac{\partial E_{\mathrm{QM}}^{\mathrm{cluster}}}{\partial r_{\mathrm{b},j}} \left(\frac{\partial r_{\mathrm{b},j}}{\partial r_{\mathrm{QM},i}}\right)_{\mathrm{CL}} \tag{7}$$

and

$$\frac{\partial E_{\mathrm{CL}}^{\mathrm{cluster}}}{\partial r_{\mathrm{QM},i}} = \left(\frac{\partial E_{\mathrm{CL}}^{\mathrm{cluster}}}{\partial r_{\mathrm{QM},i}}\right)_{\mathrm{fix}\ \{r_b\}}. \tag{8}$$

The derivatives of the energies in Eqs. (7) and (8) are obtained analytically, while the last term $(\partial r_{\mathrm{b},j}/\partial r_{\mathrm{QM},i})_{\mathrm{CL}}$ for the pair (i,j) in Eq. (7) is evaluated through explicit numerical differentiation for the buffered cluster in the CL calculation. For CL atom i, the cluster terms $E_{\mathrm{CL}}^{\mathrm{cluster}}$ and $E_{\mathrm{QM}}^{\mathrm{cluster}}$ do not contribute to the force; hence,

$$F_i = -\frac{\partial E_{\mathrm{CL}}^{\mathrm{system}}}{\partial r_{\mathrm{CL},i}}. \tag{9}$$

In the buffered-cluster method, the positions of the buffer atoms in the atomic cluster for the QM calculation are determined using the relaxed positions of the buffer atoms obtained in the CL calculation. Therefore the computation times to determine the positions of the buffer atoms for the QM calculation are negligible as compared to the DFT (i.e., QM) calculation itself. If we were to minimize the DFT energy $E_{\mathrm{QM}}^{\mathrm{cluster}}$ of the atomic cluster through relaxation of the buffer atoms in the QM calculation, there should appear various surface reconstructions of the cluster, resulting in undesirable deformations of the crystalline structure. Such a reconstruction of the surface of the cluster is suppressed in the buffered-cluster method. We in fact apply the buffered-cluster method to crystalline Si with various choices of the QM region; the total number of the QM atoms ranges from 1 to 70. We use the hybridized Hamiltonian, Eq. (1), with the buffered-cluster method and obtain the ground-state configuration by moving all the atoms until the maximum atomic force becomes smaller than 10^{-4} Ry/a.u. It is found that the maximum displacement of the atom from the crystalline position at the initial is about 0.03 Å or smaller depending on the choice of the QM region and that the maximum displacement is not sensitive to the value of β.

Let us analyze accuracies of the buffered-cluster method from mechanical and electronical points of view. The following four paragraphs explain the results of the analyses. The target system is a crystalline Si under the periodic boundary conditions; the Cartesian axes x, y, and z correspond to the $\langle 100\rangle$, $\langle 010\rangle$, and $\langle 001\rangle$ directions, respectively. The system contains the QM region of 29 Si atoms, whose close-up view is shown in Fig. 3(a), with the black spheres denoting the QM atoms. The atomic clusters for the QM and CL calculations are depicted in Figs. 3(b) and 3(c), respectively. The positions of all atoms in the total system are relaxed.

Electronic populations. We analyze how the atomic structure and the electronic populations in the QM region come to resemble those of bulk Si. We denote those QM atoms that are adjacent to the buffer atoms in the atomic cluster for the QM calculation as the outer QM atoms, the rest of the QM atoms, as the inner QM atoms. Bond lengths and Mulliken's overlap populations[32] of the Si-Si bonds in the QM region are the following. For bonds connecting between the inner QM atoms, the bond distances are 2.345 Å and the overlap populations are 0.900. The last digits fluctuate among different bonds. These values agree with the bulk values to within 1%. For bonds connecting between the outer and inner QM atoms, the bond distances are 2.392 Å and the overlap populations are 0.83. The difference in the overlap population between the two cases indicates that the strengths of the bonds that involve the outer QM atoms may differ by several percent from the bulk values. As for the Mulliken's atomic populations,[32] they are 4.00–4.09 for the inner QM atoms, while 4.17 for the outer QM atoms. Such differences of several percent in the atomic population accord with the similar degree of difference in the overlap population mentioned above. We may therefore state that few effects of the finiteness of the QM region exist in both atomic structure and electronic populations.

Local stiffness. We analyze the degree of homogeneity of mechanical stiffness in the hybridized Si system. We calculate the recoil force felt by a given atom when the atom is shifted from the equilibrium position by a given amount. Proper coupling between the QM and CL regions corresponds to agreement of the recoil forces between the QM and CL atoms in the same crystalline symmetry. Atoms 1, 2, and 3 aligning in the $\langle 101\rangle$ direction in Fig. 3(a) are equivalent in the crystal symmetry—similarly, atoms 4, 5, and 6 in the $\langle 010\rangle$ direction. Atoms 1 and 4 are located near the center of the QM region, atoms 2 and 5 at the QM-CL boundary; and atoms 3 and 6 in the CL region. Figure 4 compares the recoil force F_i on atom i as a function of the displacement dr_i from the equilibrium position in three different directions: panels (a)–(c) in Fig. 4 for the set of atoms 1, 2, and 3; panels (d)–(f) for the set of atoms 4, 5, and 6. As we see in Fig. 4, the recoil forces agree to within a few percent among atoms 1(4), 2(5), and 3(6) in all three directions of dr_i for $dr_i \leqslant 0.1$ Å. For $dr_i > 0.2$ Å, the recoil forces may differ by about 10% at most depending on the direction. The differences at large dr_i originate mainly from inaccuracy of the SW interatomic potential that we use in the present analyses, which was constructed to reproduce the elastic properties of the Si crystal at small displacements of the atoms.

Electronic states relating to dangling bonds. The buffered cluster shown in Fig. 3(b) for the QM calculation has dangling bonds on the buffer-Si atoms labeled as $\{\alpha,\beta,\gamma,\delta,\varepsilon,\phi\}$. We demonstrate that electrons corresponding to the dangling bonds are localized well on the buffer-Si atoms. Figure 5 depicts charge density on the $(10\bar{1})$ plane that contains buffer-Si atoms α and β. We observe in Fig. 5 a substantial density of the electrons at the dangling-bond sites of atoms α and β (at the left of atom α and at the right of atom β). A total of 12 electrons exist relating to the 6 buffer-Si atoms $\{\alpha,\beta,\gamma,\delta,\varepsilon,\phi\}$ in Fig. 3(b). Figure 6 (top) shows the energy levels of the KS orbitals in DFT near the Fermi level. Five doubly occupied and six unoccupied orbitals that emerge due to the existence of the dangling bonds are confirmed through visualization to be localized at the buffer-Si atoms. A contour plot of such a surface orbital just below the Fermi level is drawn in Fig. 6 (bottom), in which

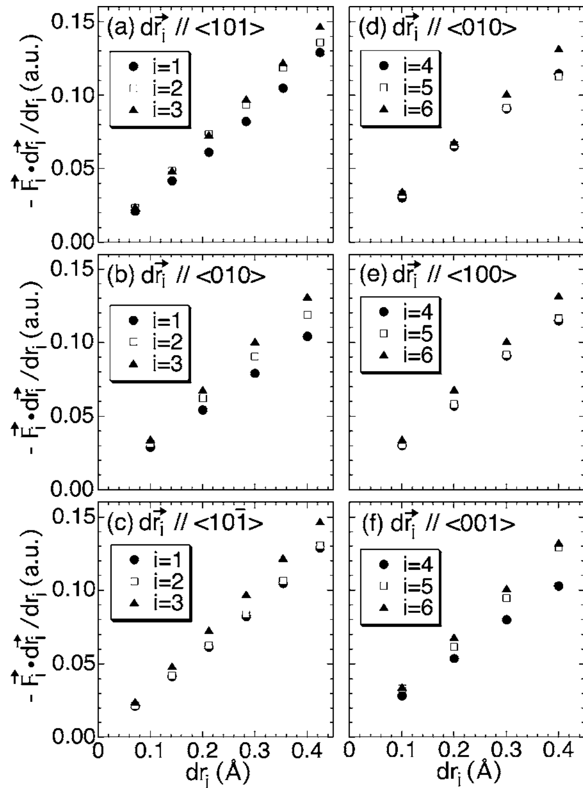

FIG. 4. Variations of the force on atom i when it is shifted by dr_i from its equilibrium position to various directions in the hybrid QM-CL simulation of crystalline Si shown in Fig. 3(a) with the buffered-cluster method. Atoms 1 and 4 are the QM atoms at around the center of the QM region, atoms 2 and 5 the QM atoms at the QM-CL boundary, and atoms 3 and 6 the CL atoms. The direction of dr_i is parallel to $\langle 101\rangle$, $\langle 010\rangle$, $\langle 10\bar{1}\rangle$, $\langle 010\rangle$, $\langle 100\rangle$, and $\langle 001\rangle$ in panels (a), (b), (c), (d), (e), and (f), respectively.

white regions mean positive values while black regions negative values. We here note that the five occupied surface states contain 10 out of 12 electrons relating to the six buffer-Si atoms and that the remaining two electrons mix with other electrons at the lower-energy states to create an additional state. If the QM region is large enough in size so that the buffer-Si atoms are separated well from the center of the region, those surface states cannot cause significant effects on the electronic structures at the center of the QM region.

Sensitivity to a Fermi-level shift. We may insert atoms in actual hybrid simulations—for instance, oxygen atoms in the oxidation simulation of a Si substrate. In those cases, the QM region should be composed of the inserted atoms and surrounding Si atoms. Relating to charge transfers between the QM atoms, the Fermi level may shift and the electronic structures of the surrounding Si may change. That is, the occupation of the surface states near the Fermi level mentioned in the previous paragraph may change by insertion of the atoms. It is hoped, for robust hybrid simulation, that the bonding characteristics between the Si atoms at the peripheral of the QM region do not change much with such a Fermi-level shift. To confirm this, we temporarily shift the Fermi level of the buffered cluster in Fig. 3(b) for the QM

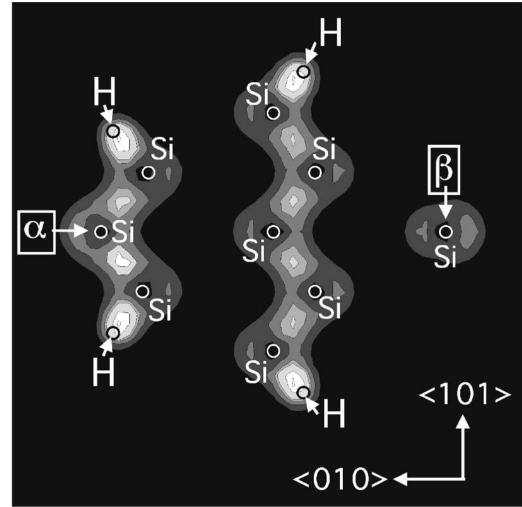

FIG. 5. Contour plot of density of the valence electrons on the lattice plane that contains atoms α and β and is perpendicular to $\langle 10\bar{1}\rangle$ obtained in the DFT (i.e., QM) calculation of the atomic cluster shown in Fig. 3(b). The higher the density, the whiter the gray scale.

calculation in the hybrid simulation so that total number of the electrons changes by −2, −1, 1, and 2. In all four cases, we relax all atoms in the total system. We thereby find that the maximum displacements of the atom due to the Fermi-

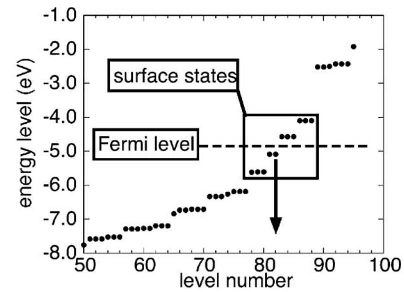

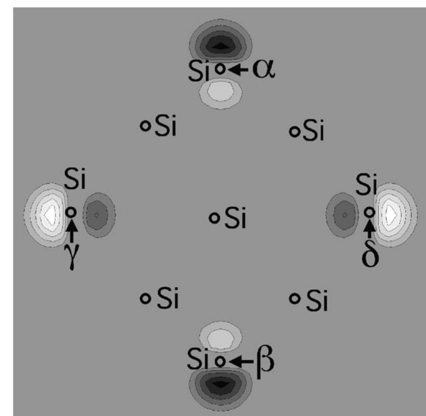

FIG. 6. (top) Diagram of the eigenvalues obtained in the DFT (i.e., QM) calculation of the atomic cluster shown in Fig. 3(b). (bottom) Contour plot of the KS orbital for the state just below the Fermi level on the lattice plane containing atoms α, β, γ, and δ obtained in the DFT calculation. The higher the value, the whiter the gray scale; zero corresponds to the gray scale of the background.

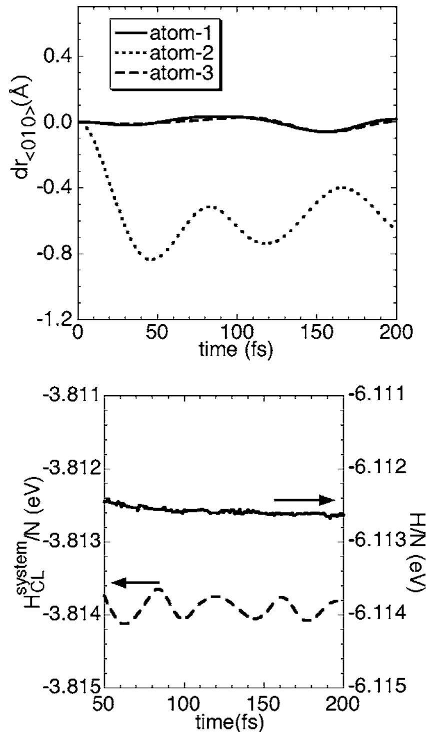

FIG. 7. (a) Time evolution of displacements of atoms 1, 2, and 3 in Fig. 3 projected to the ⟨010⟩ direction in the hybrid QM-CL simulation of crystalline Si with the buffered-cluster method. Initially atom 2 is shifted by 1.0 a.u. toward the ⟨010⟩ direction. (b) Time evolution of the total Hamiltonian H and the CL energy of the total system $H_{\rm CL}^{\rm system}$.

level shift are quite small: they are (0.025 Å, 0.013 Å, 0.0074 Å, 0.019 Å) for changes by $(-2,-1,1,2)$. Similarly, negligible variations of the atomic forces are observed in recoil-force analyses.

The total energy H in Eq. (1) with Eqs. (4) and (5) of the hybridized system should be conserved during a simulation run if the time step is small enough. A hybrid simulation run is performed with a time step of 0.67 fs starting from the configuration with atom 2 in Fig. 3(a) shifted by 1.0 a.u. from the equilibrium crystalline position toward the ⟨010⟩ direction. Figure 7 (bottom) compares the time evolutions of $H_{\rm CL}^{\rm system}/N$ and H/N. While $H_{\rm CL}^{\rm system}/N$ oscillates by about 0.0005 eV, variation of H/N is as small as 0.0001 eV, showing conservation of H/N with high accuracy. The time evolutions of positions of atoms 1, 2, and 3 during the run are depicted in Fig. 7 (top). As we see in Fig. 7 (top), the oscillatory behaviors of atoms 1 and 3 are quite similar to each other. Atom 1 belongs to the QM region and atom 3 to the CL region; atoms 1 and 3 are located at mutually symmetric positions with respect to atom 2. The similarity of the oscillatory behaviors of atoms 1 and 3 indicates homogeneity of the local stiffness in the hybridized system.

The hybrid QM-CL simulation scheme with the buffered-cluster method will be applied to various exothermic processes in materials such as the crack propagation and friction. In the hybrid simulation run of such a process, the reaction region may move and increase in size as the simulation proceeds. Adaptive rechoosing of the QM region during the simulation run will be required for fast simulation. Since virtually no limitation exists in choosing the QM region in the buffered-cluster method, automatic rechoosing of the QM region is possible during the simulation run with simple algorithms. We here give an example of the algorithm to be applied to the hybrid simulation about the reaction of an H_2O molecule with a nanostructured Si in Sec. III B. The algorithm which will be applied at a regular interval of 10 fs in the simulation run, consists of following six steps (i)–(vi).

(i) Count the coordination number (N_c) of each Si atom. Here atoms within radius of 3.1 Å (1.32 times the equilibrium bond distance) from the target atom are regarded as the coordination atoms.

(ii) (For the compressed region) If a CL-Si atom has $N_c>4$, then it is converted to the QM-Si atom.

(iii) (For the expanded region) If a CL-Si atom has $N_c=4$ and at least one of the four Si-Si distances is larger than 2.85 Å (1.2 times the equilibrium bond distance), then the atom is converted to the QM-Si atom.

(iv) Those CL-Si atoms within radius of 3.0 Å from the external atoms—e.g., O and H in H_2O in the reaction simulation—are converted to QM-Si atoms.

(v) Those CL-Si atoms located between separated QM regions are converted to QM-Si atoms. To this end, we introduce the classical hop distance (CHD) for a pair of QM-Si atoms. The CHD is defined as the minimum number of classical Si-Si bonds in which at least one of the two atoms in the bond is a CL atom, among all possible paths connecting between the two QM atoms. The CHD's for all pairs of the QM atoms are calculated. If the CHD for a pair of QM-Si atoms is larger than zero, the CL-Si atoms on the corresponding path are converted to QM-Si atoms.

(vi) Those QM-Si atoms at the peripheral of the QM region may be converted to CL-Si atoms if all four Si-Si bond lengths around the QM atom are within 10% of the equilibrium value (2.35 Å), for fast simulation.

The buffered-cluster method gives reasonable accuracies not only for covalent materials as Si in which the empirical interatomic potential is relatively short ranged but also for ionic materials such as alumina in which the empirical interatomic potential is long ranged. In the hybrid QM-CL simulation of the α-Al_2O_3 system with the buffered-cluster method, we adopt the variable-charge interatomic potential[34] for the CL calculation, in which the atoms have the effective charges determined dynamically following the generalized electronegativity equalization principles. The proper coupling between the QM and CL regions in crystalline α-Al_2O_3 is realized with the buffered-cluster method when the QM region is chosen so that the outer QM atoms (i.e., the QM atoms connecting to the CL atoms) are Al. Double layers of the buffer atoms are set in the atomic clusters for the QM and CL calculations. In the atomic cluster for the QM calculation, the first buffer layer consists of O atoms and the second buffer layer of Al and "virtual" atoms. The virtual atom has the core charge $Z_{\rm core}=0.5|e|$ with the nonintegral number 0.5 of electrons. The positions of the buffer atoms are determined from those of the buffer atoms in the atomic cluster for the CL calculation.

Figure 8(a) shows an example of the QM region chosen in crystalline α-Al_2O_3. In Fig. 8(a), the black (gray) spheres

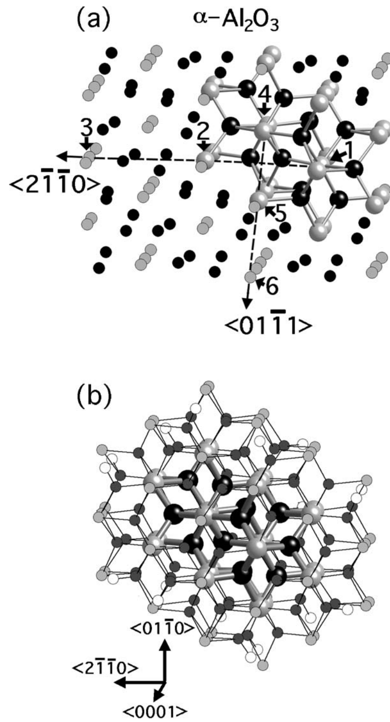

FIG. 8. (a) An example of the QM region in the hybrid QM-CL simulation of α-Al_2O_3 with the buffered-cluster method. The small spheres without shines denote the CL atoms, in which the black corresponds to Al and the gray to O. The large spheres connected mutually with the bonds denote the QM atoms, in which the black corresponds to Al and the gray to O. Atoms 1(4), 2(5), and 3(6) are equivalent in the crystalline symmetry. (b) The atomic cluster for the DFT (i.e., QM) calculation of the QM region depicted in (a) in the hybrid QM-CL simulation with the buffered-cluster method. The buffer atoms are shown by the dark-gray spheres without shines for Al atoms, the bright-gray for O atoms, and the white for the virtual atoms.

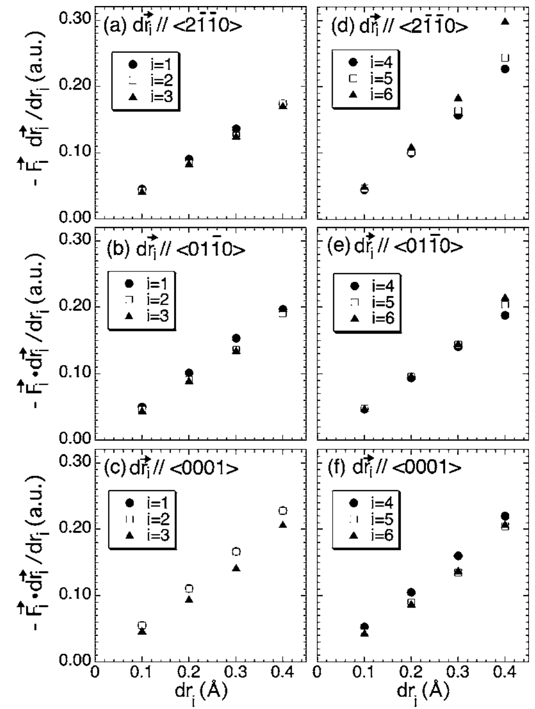

FIG. 9. Variations of the force on atom i when it is shifted by dr_i from its equilibrium position to various directions in the hybrid QM-CL simulation of α-Al_2O_3 shown in Fig. 8(a) with the buffered-cluster method. The atoms 1 and 4 are the QM atoms at around the center of the QM region, atoms 2 and 5, the QM atoms at the QM-CL boundary, and atoms 3 and 6, the CL atoms. The direction of dr_i is parallel to $\langle 2\bar{1}\bar{1}0\rangle$, $\langle 01\bar{1}0\rangle$, $\langle 0001\rangle$, $\langle 2\bar{1}\bar{1}0\rangle$, $\langle 01\bar{1}0\rangle$, and $\langle 0001\rangle$ in panels (a), (b), (c), (d), (e), and (f), respectively.

denote O (Al) atoms; the QM atoms are indicated with shines and connecting bars. The buffered atomic cluster for the QM calculation is depicted in Fig. 8(b), in which the dark-gray spheres without shines are the buffer-O atoms, the bright-gray spheres the buffer-Al atom, and the white spheres the virtual atoms. In crystalline α-Al_2O_3, each Al atom has six O atoms while each O has four Al atoms, as the coordination atoms.[34] We may temporarily call the Al-O line segment the bond, irrespective of the electronic structure. The virtual atoms are set at the broken Al-O bonds on the second buffer layer with the scaling factor β, in an analogous way to the buffer-H atom in the Si system. The β for the virtual atom is 0.57. Figure 9 shows results of the analyses of the recoil force on atom $i \in \{1,2,\ldots,6\}$ labeled in Fig. 8(a), in which atom i is shifted temporarily by dr_i from the equilibrium position in three different directions in a similar way as in the Si case in Fig. 4. Atoms 1(4), 2(5), and 3(6) in Fig. 8(a) are equivalent in the crystalline symmetry. Atoms 1 and 4 are located at around the center of the QM region, atoms 2 and 5 at the QM-CL boundary, and atoms 3 and 6 at the CL region. We thereby find in Fig. 9 that high degrees of the mechanical coupling between the QM and CL regions are realized in the hybridized α-Al_2O_3 crystal with the buffered-cluster method.

The buffered-cluster method differs from the link-atom method in two crucial points: (i) Not only H but Si is used as the buffer atom in the case of the Si system. (ii) The positions of the buffer atoms are determined by using the relaxed configuration of the corresponding buffer atoms in the CL calculation, not by referring to the positions of the HS atoms. Introduction of other species than H is necessary to reduce artificial deformation originating from mutual repulsion between the proximate H atoms in the crystalline Si system; for the α-Al_2O_3 system, H atoms cannot be used to terminate the broken bonds at the CL-QM boundary. A simple connection of the buffer-Si to the HS-Si in the Si system would result in less accuracy in the mechanical coupling between the QM and CL atoms as compared to the buffered-cluster method since the relaxed configuration of the buffer-Si differs substantially from the crystalline one and the strength of the bond between the buffer-Si and the QM-Si differs from that of the two QM-Si atoms.

In the buffered-cluster method, we have an option to saturate the buffer-Si further by H atoms for the Si system. For the α-Al_2O_3 system, however, the QM cluster cannot be saturated by, e.g., H atoms. Therefore, the buffered-cluster method without such saturation may be considered as a

simple and universal method applicable to both Si and α-Al_2O_3 systems.

We note that the long-range Coulomb interaction between the CL and QM atoms is considered through the CL potential of the total system $E_{\mathrm{CL}}^{\mathrm{system}}$ [see Eq. (1)]. For the Si system, the SW potential that we adopt has no atomic charges and hence the Coulomb interaction is ignored in practice. For the α-Al_2O_3 system, the Coulomb interaction is calculated with the atomic charges in the variable-charge potential,[34] which vary dynamically.

III. APPLICATION: REACTION OF H_2O WITH NANOSTRUCTURED SILICON

The hybrid QM-CL simulation scheme with the buffered-cluster method may be applied usefully to various phases of atomistic processes of engineering interests in nanostructured materials. The MEMS is a complex nanosystem composed of electronic and mechanical components in submicrometer ranges, which is made of a Si-based material and fabricated using semiconductor processing techniques such as directional etching. Despite the growing expectation of its usage in sensing, control, and medical applications, the MEMS may exhibit unwanted failure due to the accelerated corrosion resulting from high-frequency stress variations of the components. For instance, while the stress corrosion cracking is not observed for the bulk Si in an oxidizing environment, it is observed[21] for Si-MEMS. Since the MEMS is expected to be used in mission-critical applications, its lifetime prediction is crucial. Theoretical understanding of chemical reactions of environmental molecules with nanostructured Si systems under stresses will be useful in designing the MEMS.

The stress dependence of the oxidation reaction of Si is also a principal theme of active researches, with the intention of exploiting the information to realization of advanced computer and memory chips. A CMOS field-effect transistor (FET) with gate SiO_2 length on the order of 10^0 nm, corresponding to several atomic layers, has been targeted. The gate dielectrics of the FET are usually produced through the wet oxidation or the deposition processes. Controlled production of such an ultrathin oxide layer requires detailed knowledge about the dissociation and oxidation processes of water molecules on the nanostructured Si under various external stresses relating to the three-dimensional fine structures of the system.

Motivated by those, in the present section, we study the initial stages of the H_2O reaction with a nanostructured Si using the hybrid QM-CL simulation scheme with the buffered-cluster method. The initial stages include adsorption and dissociation processes of the H_2O molecule on the Si system, which may vary qualitatively depending on the degree of strain applied to the system. We will consider a notched Si-slab system with the bottom facet of the notch assuming the Si(100)-(2×1) dimer structure and will put an H_2O molecule above the facet. In Sec. III A, we will calculate the potential energy as a function of the distance between the H_2O and the facet using the hybrid QM-CL simulation with the buffered-cluster method. Both strained and unstrained systems will be considered to understand the dependence of the adsorption energy on the strain. Since those static data are not enough to predict the reaction dynamics, we will perform the hybrid QM-CL simulation for reaction dynamics of the H_2O molecule with the nanostrucutured Si in Sec. III B.

A. Static analyses

We prepare a Si-slab system with dimensions $(L_x, L_y, L_z) = (108.6\ \text{Å}, 27.1\ \text{Å}, 70.6\ \text{Å})$. Periodic boundary conditions are assumed in the x and y directions, while the free-boundary condition in the z direction. The diamond crystalline structure is assumed to the system; the x axis corresponds to the $\langle 1\bar{1}0\rangle$ direction, y axis to $\langle 110\rangle$, and z axis to $\langle 001\rangle$. Then a notch with x width ~ 16 Å and z height ~ 36 Å is inserted at the middle of the system. The bottom of the notch assumes a facet with (001) structure and two sidewalls of the notch with $(1\bar{1}0)$ structure. Additionally, facets with (111) structure are created at the corners between the bottom and the two sidewalls of the notch, which act to stabilize the initial crystalline configuration around the corners. We prepare another system by removing one more atomic layer from the bottom of the notch in the Si-slab system explained above. In both systems, we initially create symmetric (1×1) Si-Si dimers on the bottom of the notch and then perform a MD simulation with the velocity dumping method using the SW interatomic potential to obtain the relaxed atomic configuration. The dimers are perpendicular to the x direction in one system, while they are perpendicular to the y direction in the other system.

To prepare stretched systems we first expand both systems uniformly by 4% in the x direction and then relax their atomic positions by the MD simulation with the velocity dumping method until the maximum atomic force becomes smaller than 10^{-4}Ry/a.u. To characterize stress distributions in the stretched systems, we draw the atomic virial stresses[35] σ_{xx} in the systems in Fig. 10: (a) for the system with the dimers oriented perpendicularly to the x direction and (b) for the system to the y direction. In the stretched systems, a stress concentration is observed at the bottom of the notch. The maximum magnitude of σ_{xx} is about 8 GPa at the center of the notches in the stretched system, which is about 4 times larger than the averaged magnitude of 2 GPa at the low-x and high-x ends of the system. Interestingly stress variations near the bottom of the notch differ significantly between the two systems as seen in Figs. 10(a) and 10(b), which is a reflection of different combinations of the stretch and dimer directions between the two systems.

Up to this point, we have four different systems. In two of the four systems the dimers are perpendicular to the x direction; one is the unstrained system, the other is the stretched system in the x direction. In the other two systems, the dimers are perpendicular to the y direction; one is the unstrained system, the other is the stretched system in the y direction. Since atomic configurations at the center of the notch bottom in the two unstrained systems are the same, we choose to consider the following three systems: (i) the unstrained system with the dimers oriented perpendicularly to

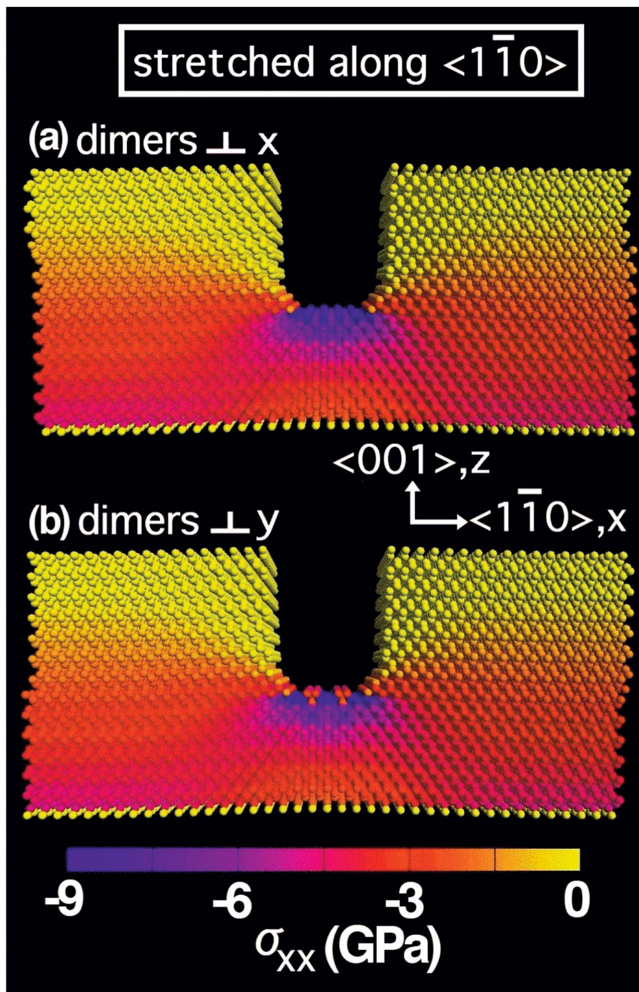

FIG. 10. (Color) The atomic virial stresses σ_{xx} in the 4%-stretched Si system with the notch obtained with the classical MD simulation. (a) For the system with Si-Si dimers at the bottom of the notch oriented perpendicularly to the x direction. (b) For the system with Si-Si dimers at the bottom of the notch oriented perpendicularly to the y direction.

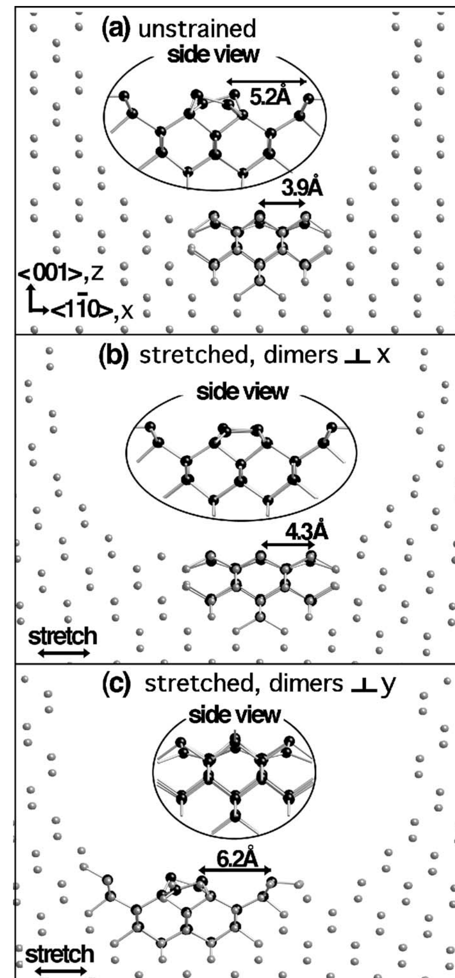

FIG. 11. (a) Close-up view of the QM region in the hybrid QM-CL simulation of the unstrained Si system containing the notch with the buffered-cluster method; the black spheres correspond to the QM-Si atoms. (b) Same as (a) but for the 4%-stretched Si system with dimers at the bottom of the notch oriented perpendicularly to the x direction. (c) Same as (a) but for the 4%-stretched system with dimers at the bottom of the notch oriented perpendicularly to the y direction.

the x direction, (ii) the stretched system with the dimers oriented perpendicularly to the x direction, and (iii) the stretched system with the dimers oriented perpendicularly to the y direction. For each of the three systems, we choose the QM region at the bottom of the notch and perform the hybrid QM-CL simulation run with the velocity dumping for structural relaxation until the maximum atomic force becomes smaller than 10^{-4} Ry/a.u. Figure 11 depicts the QM regions with the surrounding Si atoms: (a) for the unstrained system, (b) for the stretched system with the dimers oriented perpendicularly to the x direction, and (c) for the stretched system with the dimers oriented perpendicularly to the y direction. In Fig. 11, the small spheres denote the CL-Si atoms, while the large spheres the QM-Si atoms; bonds are drawn to guide the eye. We observe in Fig. 11(a) the formation of buckling (2×1) dimer structure on the bottom of the notch in the same way as has been observed on the Si(100) surface.[36] We note that stretching the notched system acts to weaken the degrees of the buckling and that the buckling almost disappears in Fig. 11(b) in which the dimers are perpendicular to the stretch direction (i.e., x direction). The disappearance has resulted since an increase in the interdimer distance by about 10%, from 3.9 Å to 4.3 Å depicted in Figs. 11(a) and 11(b), flattens the up-down behavior of the dimer atoms in the z direction without changing lengths of the Si-Si bonds in the dimers significantly. The 10% increase in the interdimer distance, which is substantially larger than 4% of the system stretching, is related to the stress concentration at the bottom of the notch (see Fig. 10).

1. Adsorption of H_2O

It is well known[37] that the H_2O molecule adsorbs to the down atom of the Si-Si dimer on Si(100) surface to form the Si-O bond. We add an H_2O molecule to the QM region in the hybridized system shown in Fig. 11. The total potential energy of the hybrid system is minimized using the hybrid

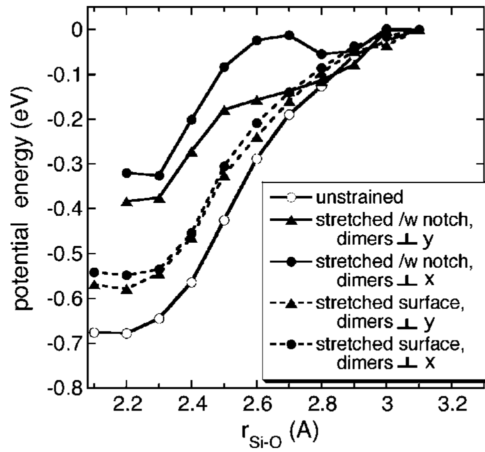

FIG. 12. Variations of the potential energy as a function of the distance $r_{\mathrm{Si}=\mathrm{O}}$ between the O atom in H_2O and the down atom of the Si-Si dimer on the (100) facet obtained in the hybrid QM-CL simulation of various Si systems with the buffered-cluster method. Solid curves with open circles, triangles, and solid circles correspond to the unstrained system [see Fig. 11(a)], the stretched system with the notch in which dimers are perpendicular to the *y* direction [see Fig. 11(c)], and the stretched system with the notch in which dimers are perpendicular to the *x* direction [see Fig. 11(b)], respectively. The dashed curves with triangles and circles correspond to the stretched surfaces with dimers oriented perpendicularly to the *y* and *x* directions, respectively.

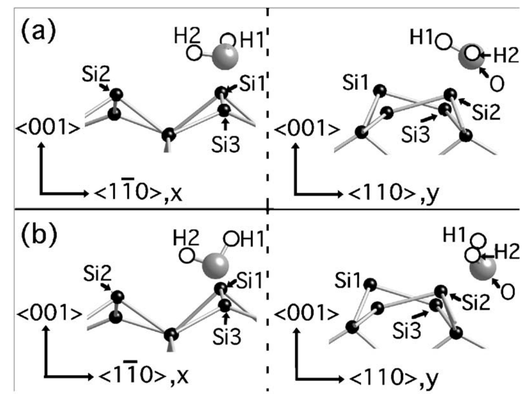

FIG. 13. (a) Close-up views of the atomic configuration of the H_2O-adsorbed Si(100) facet in the unstrained Si system at the ground state. (b) Same as (a) but of the atomic configuration at the metastable state.

simulation scheme with the buffered-cluster method under the constraint of fixing the Si-O distance $r_{\text{Si-O}}$. Before starting detailed analyses of the potential energy profile, we have separately checked the dependence of the force felt by the O atom on the size of the QM region when the H_2O is set at $r_{\text{Si-O}}=2.8$ Å. We have considered two different sizes, 33 and 61 Si atoms, of the QM region, to find only a 5% difference in the force. We have therefore judged that the present choice of QM region containing 33 Si atoms is appropriate. We decrease $r_{\text{Si-O}}$ in a stepwise manner starting from $r_{\text{Si-O}}=3.1$ Å; the total potential energy is calculated at each $r_{\text{Si-O}}$ with relaxation of the atomic positions.

In Fig. 12, we plot the total potential energies of the three hybridized systems as functions of $r_{\text{Si-O}}$ with the solid curves. The zero-energy state is set to the case of $r_{\text{Si-O}}=3.1$ Å. For the unstrained system, we obtain the adsorption energy of about 0.7 eV, in agreement with the known value[38,39] for the Si(100) surface, as plotted in Fig. 12 by the solid curve with open circles. Close-up views of the atomic configuration at the adsorption state are shown in Fig. 13(a) for the unstrained system. Distances between the atoms are $d(\text{O-Si3})=2.11$ Å, $d(\text{Si1-H1})=2.87$ Å, and $d(\text{Si2-H2})=3.16$ Å; the overlap populations are $p(\text{Si1-H1})=0.16$ and $p(\text{Si2-H2})=0.13$. Therefore weak bonds are formed for the pairs Si1-H1 and Si2-H2 in Fig. 13(a), which is reasonable since dangling bonds exist at Si1 and Si2. We observe in Fig. 12 substantial dependences of the adsorption energy on the strain applied to the notched systems; the adsorption energies become about a half, 0.3–0.4 eV, due to the stretching. For the stretched system with the notch in which the dimers are perpendicular to $\langle 1\bar{1}0\rangle$—i.e., the *x* direction—the energy curve in Fig. 12 has a local minimum at $r_{\text{Si-O}}=2.9$ Å. It is known that buckling of the dimer is essential for the H_2O molecule to adsorb to Si(100) surface. As we have seen in Fig. 11, the buckling almost disappears when the system with the dimers oriented perpendicularly to the *x* direction is stretched by 4% in the *x* direction. A slight variation in the buckling behavior has created the local-minimum structure in the energy profile in Fig. 12. As references, we plot additionally in Fig. 12 variations of the total potential energies in the cases of Si(100) surfaces with uniform stretching by 4% in the *x* direction; the dimers are perpendicular to either the *x* (the dashed curves with closed circles in Fig. 12) or *y* (the dashed curves with closed triangles) direction. In the surface systems, no stress concentration exists and hence relatively small modifications of the adsorption energy result from the 4% stretching.

After we have obtained the adsorption state of the H_2O at $r_{\text{Si-O}}=2.1$ Å in the unstrained system, we search metastable states around the adsorption state. Figure 13(b) depicts the metastable state found in the unstrained system. For the stretched systems with the notch, we do not find such a metastable state. The metastable state in the unstrained system is 0.3 eV higher in the potential energy than the adsorption state; the metastable state has a shallow energy barrier of 0.1 eV along the path toward the adsorption state in Fig. 13(a). At the metastable state, interatomic distances are $d(\text{O-Si3})=2.17$ Å, $d(\text{Si1-H1})=4.14$ Å, and $d(\text{Si2-H2})=3.00$ Å; the overlap populations are $p(\text{Si1-H1})=-0.02$ and $p(\text{Si2-H2})=0.14$. The weak bond between Si1 and H1 atoms observed at the adsorption state in Fig. 13(a) is broken at the metastable state in Fig. 13(b), which is accompanied by a slight increase in the degree of bonding between Si2 and H2 atoms.

2. Dissociation of H_2O

In the previous subsection we have found that the adsorption energy of H_2O decreases significantly when the notched Si system is stretched. It is known that the H_2O molecule dissociates and that the resulting fragments (H and OH) adsorb to the dangling-bond sites of the dimers on Si(100)

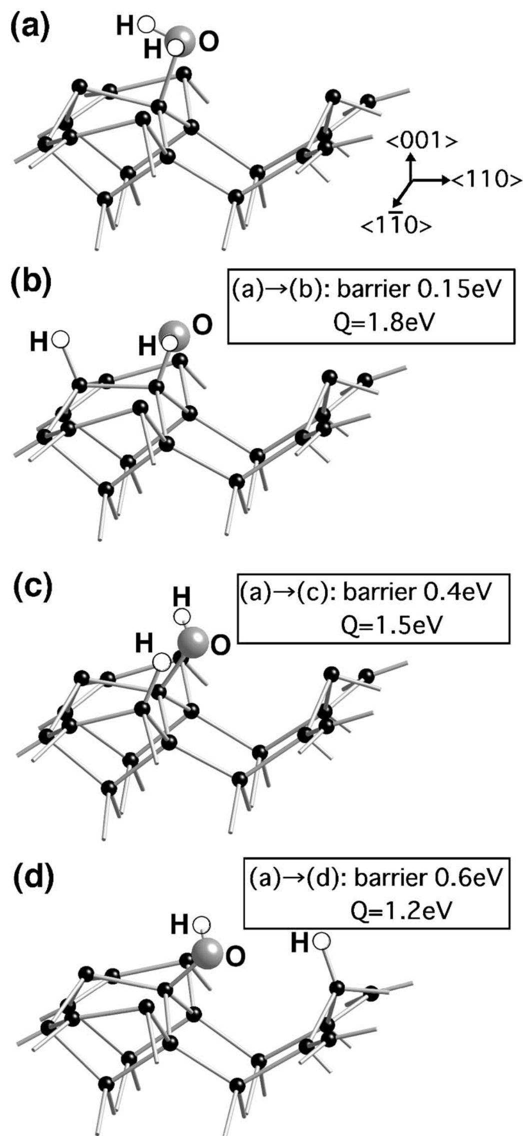

FIG. 14. (a) Atomic configuration of the H_2O-adsorbed Si(100) facet in the unstrained Si system. (b) The dissociated state with H and OH adsorbed to the same Si-Si dimer. (c) The dissociatied state with H adsorbed to the first-nearest-neighbor dimer. (d) The dissociated state with H adsorbed to the second-nearest-neighbor dimer.

surface when the surface is exposed to a moisture environment.[40–43] Since a plural number of the dimers exist in the vicinity of the adsorption site of Si(100), various dissociation processes can be imagined. The dissociation process involving a single dimer on Si(100) has been considered to be the most probable.[38,39] It is interesting to compare the energy barriers and the dissociation energies of various dissociation processes with their dependences on the strain applied to the system.

We depict in Fig. 14 three dissociation processes of the adsorbed H_2O at the bottom facet of the notch with Si(100)-(2$\times$1) dimer structure in the unstrained Si system. The configuration of the QM atoms chosen in the hybrid simulation is depicted in Fig. 14(a) for the adsorbed state, in Figs. 14(b)–14(d) for the three dissociated states. Since the direct interaction between the H_2O and the sidewalls of the notch is ignored in the present choice of the QM region, such a simulation for the unstrained Si system may correspond to considering a Si(100) surface. The three processes considered are dissociation on the same dimer—that is, from (a) to (b) in Fig. 14; dissociation to the first nearest-neighbor dimer, from (a) to (c); and dissociation to the second nearest-neighbor dimer, from (a) to (d).

In the case of the dissociation on the same dimer, we perform the hybrid simulation of atomic relaxation with the constraint of fixing the distance between the H and Si atoms of the dimer. By decreasing the Si-H distance in a stepwise manner we find that the energy barrier is 0.15 eV and the dissociation energy from the adsorbed state is $Q=1.8$ eV, in agreement with the value in Ref. 38. In the case of the dissociation to the first-nearest neighbor dimer, the barrier is 0.4 eV and the dissociation energy is $Q=1.5$ eV. In the case of the dissociation to the second-nearest-neighbor dimer, the barrier is 0.6 eV and the dissociation energy is $Q=1.2$ eV.

From the thermodynamic point of view, the small barrier and large dissociation energy Q are favorable for the dissociation process to occur. We find through the explicit calculations mentioned above that the dissociation process on the same dimer corresponds to the case with the smallest barrier and the largest Q. The fact does not necessarily mean that the dissociated fragments (H and OH) adsorb always to the same dimer. We recall that the adsorbed H_2O may have a kinetic energy of 0.7 eV, which is larger than or nearly equal to the barriers of 0.15, 0.4, and 0.6 eV for the three dissociation processes considered. We may expect that all the three dissociation processes may occur depending on the initial settings.

We perform similar analyses of the dissociation processes of the adsorbed H_2O on the 4%-stretched Si systems with the notch. For the stretched system with the dimers oriented perpendicularly to the x direction [see Fig. 11(b)], we obtain the barriers of 0.05, 0.6, and 0.6 eV and dissociation energies $Q=1.6$, 1.4, and 0.4 eV for dissociations on the same dimer, to the first-nearest-neighbor dimer and to the second-nearest-neighbor dimer respectively. For the stretched system with the dimers oriented perpendicularly to the y direction, the barriers are 0.1, 0.4, and 0.8 eV and the dissociation energies are $Q=1.7$, 1.5, and 0.5 eV for dissociations on the same dimer, to the first-nearest-neighbor dimer and to the second-nearest-neighbor dimer, respectively. The barrier for the dissociation on the same dimer decreases when the system is stretched, while it increases for the other two processes. The increases in the barrier can be understood by remembering that the interdimer distances increase significantly due to the stretching, as depicted in Fig. 11. Only in the dissociation process on the same dimer are the adsorption energies ranging 0.3–0.4 eV larger than the barriers ranging 0.05–0.1 eV. We therefore expect that dissociation of H_2O will occur with high probabilities on the same dimer in the 4%-stretched Si systems with the notch. In the next subsection we will perform hybrid simulation runs to investigate the dynamics of the adsorption and dissociation processes of H_2O on notched Si systems with or without strains.

B. Reaction dynamics

As we have explained in Sec. III A, all three dissociation processes [from (a) to (b), from (a) to (c), and from (a) to (d)

in Fig. 14] may occur in the unstrained Si system from the viewpoint of thermodynamics. Such energy-based considerations cannot predict the dissociation dynamics and the resulting final states. One might guess that dissociation to the second-nearest-neighbor dimer occurs with a negligible probability from following reasons. For the process to occur, detailed conditions about the internal coordinates of the H_2O such as the rotational angles and the bond lengths need be matched with the conditions at the transition state since the adsorption energy ($\sim$0.7 eV) and barrier ($\sim$0.6 eV) are similar. If the conditions do not match, the kinetic energy $\sim$0.7 eV of the H_2O will diffuse to the surrounding atoms. Considering the Arrhenius-type thermal activation processes, we may predict that the adsorbed H_2O will dissociate readily at $\sim$100 K only through the dissociation process on the same dimer (the barrier is 0.15 eV). Here an attempt frequency of $\sim 10^{13}$ Hz is assumed.

If the dissociation to either the first-nearest-neighbor or second-nearest-neighbor dimer occurs with finite probabilities, the H_2O-exposed Si(100) surface would have a large fraction of partially saturated dimers at the initial stage. Detailed processes of the dissociative adsorption of water molecules have attracted much attention because of their importance in wet oxidation in silicon-based device technology. The oxidation barrier for the Si-Si dimer with only a single OH adsorbed to one of two dangling-bond sites has been calculated to be[44] $\sim$2.1 eV, which is smaller by 0.3 eV than the corresponding value[44,45] for the case with both H and OH adsorbed to each of the two dangling-bond sites of the Si -Si dimer. It means that the oxidation processes are promoted substantially by the existence of a dangling bond on the OH-adsorbed dimer. The dissociative adsorption of H_2O on modified Si(100) surfaces that are partially saturated by the water fragments—i.e., H and OH—has also been investigated,[39] to find that the dissociation becomes smaller than that on a clean surface. It is therefore interesting to investigate through theoretical simulation if the dissociation to either the first-nearest-neighbor or second-nearest-neighbor dimer occurs in realistic settings and its dependence on the applied stress. We will perform the hybrid QM-CL simulation runs of the H_2O reaction with the notched Si system with or without strains. It is essential to have both reacting atoms and surrounding atoms in realistic settings. We will show that dissociation to the second-nearest-neighbor dimer in fact occurs in the unstrained system.

The simulation systems are the same as have been used in Sec. III A for analyses of the energy profile; both unstrained and 4%-stretched Si systems with the notch are considered. The QM region chosen in the system contains 33 Si atoms and a single H_2O molecule. The H_2O is set above the down atom of a Si-Si dimer on the bottom facet of the notch with $r_{\text{Si-O}}=3.1$ Å. The positions of all atoms are relaxed with the constraint of $r_{\text{Si-O}}=3.1$ Å. Figures 15(a) and 18(a) show the initial configurations of the QM atoms in the unstrained and the 4%-stretched Si systems, respectively: the black, the white, and the gray spheres correspond to Si, H, and O atoms, respectively.

For the unstrained system with the notch, we perform five simulation runs with different initial velocities for the H_2O

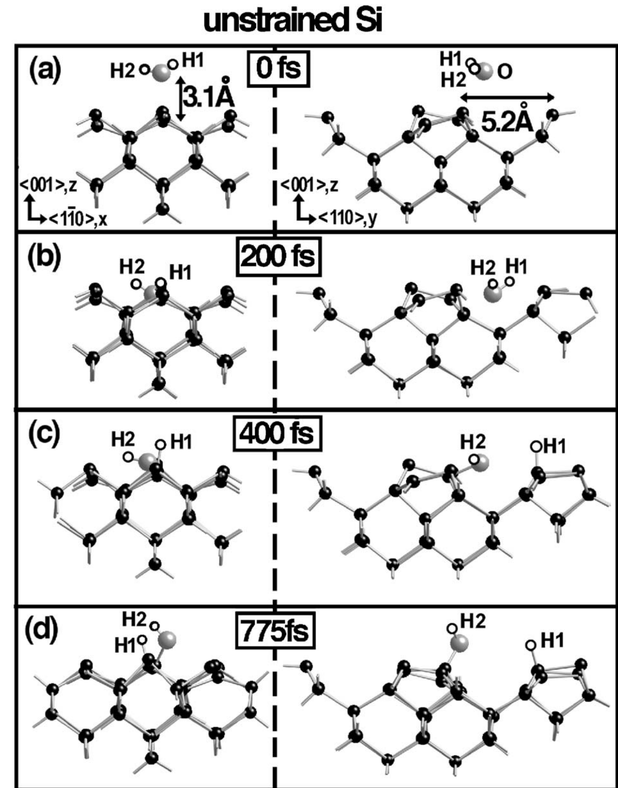

FIG. 15. Time evolution of configuration of the QM atoms in the hybrid QM-CL simulation of the dissociation process of H_2O in the unstrained Si system with the buffered-cluster method.

molecule. We set the same velocity v to 2H and O atoms of the H_2O; the magnitude of v corresponds to temperature T =600 K of the O atom—i.e., $\frac{1}{2}m_{\text{O}}v^2=\frac{3}{2}k_{\text{B}}T$. The initial velocities in the five runs are $(v_x,v_y,v_z)=(0\text{ m/s},0\text{ m/s},-680\text{ m/s})$, $(0\text{ m/s},-200\text{ m/s},-650\text{ m/s})$, $(0\text{ m/s},200\text{ m/s},-650\text{ m/s})$, $(-200\text{ m/s},0\text{ m/s},-650\text{ m/s})$, and $(200\text{ m/s},0\text{ m/s},-650\text{ m/s})$. Since the O and H atoms move during the simulation run, expansion of the QM region becomes necessary. We apply the algorithm explained in Sec. II at every 10 fs to rechoose the QM atoms adaptively in the total system. Step (iv) in the algorithm, which decreases the number of the QM atoms, is skipped in the present simulation. The time step is 0.67 fs. No temperature control is performed. In two of the five runs, we find that the H_2O dissociates to H and OH and that H adsorbs to a dangling-bond site of the second nearest-neighbor dimer, which corresponds to the process from (a) to (d) in Fig. 14. In the other three runs, the H_2O adsorbs simply to a dangling-bond site of the dimer without dissociation.

The time evolution of the atomic configuration in the dissociation run of the unstrained system with $(v_x,v_y,v_z)=(0\text{ m/s},0\text{ m/s},-680\text{ m/s})$ is depicted in Fig. 15. The QM region expands at 40, 70, 210, 390, and 450 fs with addition of 2, 1, 3, 3, and 3 QM-Si atoms, respectively, as the simulation proceeds. Figure 16(a) shows the time evolution of the averaged value of the kinetic energies of the three atoms (2H and O) in the dissociation run and, correspondingly, the Mulliken charges of the atoms in Fig. 16(b). As we observe in

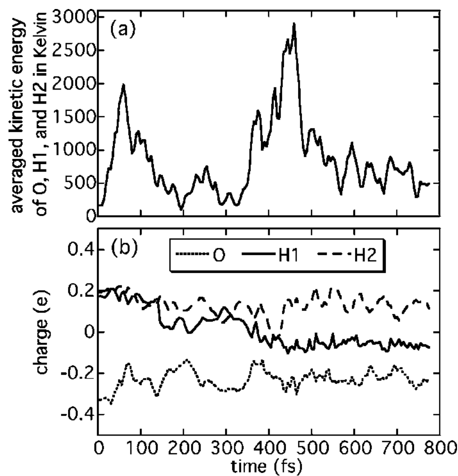

FIG. 16. (a) Time evolution of the averaged kinetic energy of O, H1, and H2 atoms in energy units in the hybrid QM-CL simulation of the dissociation process of H_2O in the unstrained Si system depicted in Fig. 15. (b) Same as (a) but of the Mulliken charges of the atoms.

Figs. 15 and 16, the H_2O molecule collides with the down atom of the dimer and starts bouncing at 80 fs; then the molecule approaches the transition state of the dissociation process to the second-nearest-neighbor dimer and takes almost zero velocities at 200 fs; finally a single H atom dissociated from the H_2O adsorbs to a dangling bond of the second-nearest-neighbor dimer at 400 fs. The kinetic energies of the three atoms (2H and O) diffuse gradually to the surrounding atoms. Such low velocities of the three atoms observed at 200 fs in Fig. 16(a) have resulted since the adsorption energy is similar to the barrier in the dissociation process to the second-nearest-neighbor dimer. The Mulliken charge of H1 becomes negative when H1 adsorbs to the dangling bond and forms the Si-H bond at 400 fs as seen in Fig. 16(b). Separately we perform a hybrid simulation run for a similar unstrained Si system with increased x width $\sim$40 Å of the notch. We use the same initial settings of $r_{\text{Si-O}}=3.1$ Å and $(v_x,v_y,v_z)=(0\ \text{m/s},0\ \text{m/s},-680\ \text{m/s})$ to understand possible effects of the two sidewalls of the notch on the dissociation process through diffusion of the reaction heat. The same dissociation process of the H_2O to the second-nearest-neighbor dimer is then observed, indicating insensitivity to the location of the sidewalls.

Snapshots of the configuration of the QM atoms in the adsorption run of the unstrained system with $(v_x,v_y,v_z)=(0\ \text{m/s},200\ \text{m/s},-650\ \text{m/s})$ are depicted in Fig. 17. The QM region expands at 40, 60, 70, and 250 fs with the addition of 2, 1, 2, and 2 QM-Si atoms, respectively. As we see in Fig. 17, the H_2O molecule collides with the down atom of the dimer and then approaches the transition state at 200 fs in a similar way as in the dissociation run in Fig. 15. The H_2O molecule is unable to pass the transition state and returns back to the adsorption state. Oscillatory behavior of the H_2O molecule with transitions between the adsorption state [see Fig. 13(a)] and metastable state [see Fig. 13(b)] is observed at times after 300 fs.

We investigate the dependence of the reaction dynamics of the H_2O molecule with the notched Si system on the strain applied to the system. We consider two 4%-stretched Si systems with the notch; dimers on the bottom of the notch are perpendicular to the x direction in one system, while they are perpendicular to the y direction in the other system. Initially the H_2O molecule is set at $r_{\text{Si-O}}=3.1$ Å above the down atom of a dimer, in a similar way to the case of the unstrained Si system. For each system, we perform five simulation runs with the same initial velocities of the H_2O molecule as that in the simulation runs for the unstrained system. In all runs, we find that the H_2O molecule approaches the down atom of the dimer and dissociates and that the resulting H and OH adsorb to the same dimer. Figure 18 depicts close-up views of the QM region in the stretched system at the initial and 120 fs. At the initial, the dimers are perpendicular to the x direction and the velocity of the H_2O is $(v_x,v_y,v_z)=(0\ \text{m/s},0\ \text{m/s},-680\ \text{m/s})$. The QM region expands at 40 fs with addition of one QM-Si atom. Since the barriers of the H transfer toward nearby dimers increase substantially in the stretched system, the dissociation of the H_2O molecule on the same dimer has resulted.

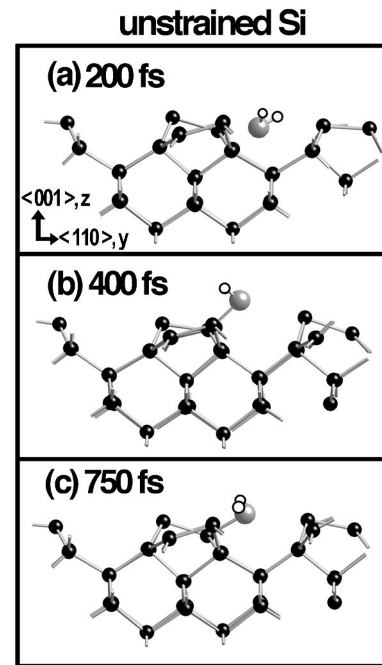

FIG. 17. Time evolution of configuration of the QM atoms in the hybrid QM-CL simulation of the adsorption process of H_2O in the unstrained Si system with the buffered-cluster method. The Si -O distance is $r_{\text{Si-O}}=3.1$ Å at the initial.

Through a series of hybrid simulation runs mentioned above, we have demonstrated that the H atom dissociated from the H_2O molecule has substantial probabilities to adsorb to a nearby dimer in the unstrained Si systems. Stretching the notched system lowers the probabilities of H adsorption to a nearby dimer.

IV. CONCLUDING REMARKS

In this paper we have demonstrated the limited applicability of the link-atom method in the hybrid QM-CL simula-

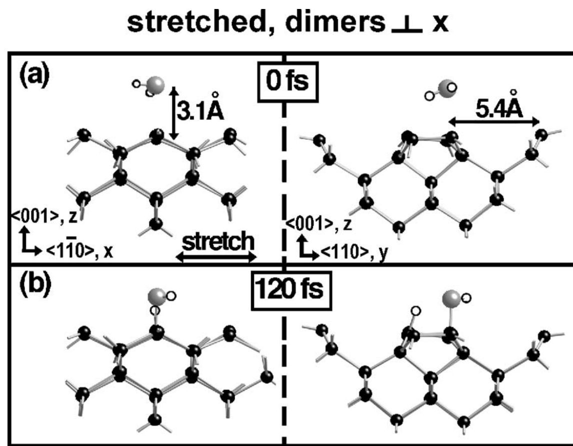

FIG. 18. Time evolution of configuration of the QM atoms in the hybrid QM-CL simulation of the dissociation process of H_2O in the 4%-stretched Si system with the buffered-cluster method. At the initial, the Si-Si dimers are perpendicular to x direction and $r_{\text{Si-O}}$ =3.1 Å.

tion scheme. For the Si system, H atoms are used in the link-atom method for termination of the broken Si-Si bonds at the QM-CL boundary. Depending on the choice of QM region in the crystalline Si system, the termination-H atoms may approach too close to each other, resulting in significant deformation of the crystalline configuration at the QM-CL boundary. To overcome this problem, we have proposed the buffered-cluster method to couple the QM and CL regions, which is applicable to any reasonable choice of QM region in a wide range of ceramics and semiconductor materials. The accuracies of the buffered-cluster method have been analyzed by applying it to crystalline Si and alumina systems. We have thereby found little differences between the QM and CL atoms in the same crystalline symmetry in respect to the equilibrium positions and recoil forces of the atoms. The insensitivity of the buffered-cluster method to the choice of QM region makes it possible to rechoose the QM region adaptively during the simulation run for fast simulations.

The buffered-cluster method has been applied to adsorption and dissociation of an H_2O molecule on the notched Si-slab system. The QM region has been chosen to include the reaction region, and the molecule has reacted with the bottom facet of the notch with Si(100)-(2×1) dimer structure. We have found that the adsorption and dissociation energies of the H_2O molecule with Si(100) facet are sensitive to the strain applied to the system. The adsorption energy decreases, while the dissociation barrier with H transferred to a nearby dimer increases, when the system is stretched. The hybrid simulation runs with the buffered-cluster method have been performed to study the dynamics of the adsorption and dissociation of the H_2O molecule on the notched Si-slab system under both stretched and unstrained conditions. In the simulation run, the QM region has changed adaptively to trace the reaction processes. The dissociation probability of the H_2O molecule and the resulting H-transfer path have depended significantly on both the strain and initial settings of the molecule, demonstrating the importance of taking into account realistic conditions in the simulation. We have demonstrated that the H atom dissociated from the H_2O molecule has substantial probabilities to adsorb to the neighboring dimer in unstrained Si systems and high probabilities to adsorb to the same dimer in stretched systems.

ACKNOWLEDGMENTS

The author would like to thank Professor A. Nakano, Dr. R. Belkada, and Dr. T. Igarashi for useful discussions. This work was supported by ACT-JST "Development of hybrid quantum-classical simulation schemes on computation grids" and a Grant-in-Aid for Scientific Research of the Ministry of Education, Science, Sports, and Culture of Japan (No. 16605005).

[1] E. Meyer, R. M. Overney, K. Dransfeld, and T. Gyalog, *Nanoscience: Friction and Rheology on the Nanometer Scale* (World Scientific, Singapore, 1999), p. 349.
[2] IEEE, *Microelectromechanical Systems (MEMS), 1999 IEEE 12th International* (IEEE, New York, 1999).
[3] C. M. Mate, G. M. McClelland, R. Erlandsson, and S. Chiang, Phys. Rev. Lett. **59**, 1942 (1987).
[4] T. L. Anderson, *Fracture Mechanics*, 2nd ed. (CRC Press, New York, 1995).
[5] *Nanoparticles and Nanostructured Films*, edited by J. H. Fendler (Wiley-VCH, New York, 1998).
[6] Y.-M. Chiang, D. Birnie III, and W. D. Kingery, *Physical Ceramics* (Wiley, New York, 1997).
[7] A. Nakano, M. E. Bachlechner, P. Branicio, T. J. Campbell, I. Ebbsjö, R. K. Kalia, A. Madhukar, S. Ogata, A. Omeltchenko, J. P. Rino, F. Shimojo, P. Walsh, and P. Vashishta, IEEE Trans. Electron Devices **47**, 1804 (2000).
[8] A. Nakano, M. E. Bachlechner, R. K. Kalia, E. Lidorikis, P. Vashishta, G. Z. Voyiadjis, T. J. Campbell, S. Ogata, and F. Shimojo, Comput. Sci. Eng. **3**, 56 (2001).
[9] G. Lu and E. Kaxiras, in *Handbook of Theoretical and Computational Nanotechnology*, edited by M. Rieth and W. Schommers (American Science, New York, 2005), Vol. X, Chap. 22.
[10] J. Q. Broughton, F. F. Abraham, N. Bernstein, and E. Kaxiras, Phys. Rev. B **60**, 2391 (1999).
[11] P. Hohenberg and W. Kohn, Phys. Rev. **136**, B864 (1964).
[12] W. Kohn and L. J. Sham, Phys. Rev. **140**, A1133 (1965).
[13] M. C. Payne, M. P. Teter, D. C. Allan, T. A. Arias, and J. D. Joannopoulos, Rev. Mod. Phys. **64**, 1045 (1992).
[14] M. Eichinger, P. Tavan, J. Hutter, and M. Parinello, J. Chem. Phys. **110**, 10452 (1999).
[15] S. Ogata, E. Lidorikis, F. Shimojo, A. Nakano, P. Vashishta, and R. K. Kalia, Comput. Phys. Commun. **138**, 143 (2001).
[16] S. Ogata, F. Shimojo, R. K. Kalia, A. Nakano, and P. Vashishta, Comput. Phys. Commun. **149**, 30 (2002).
[17] J. R. Chelikowsky, N. Troullier, and Y. Saad, Phys. Rev. Lett. **72**,

1240 (1994).
[18] F. Shimojo, T. J. Campbell, R. K. Kalia, A. Nakano, S. Ogata, P. Vashishta, and K. Tsuruta, Future Gen. Comp. Sys. **17**, 279 (2000).
[19] S. Ogata, F. Shimojo, A. Nakano, P. Vashishta, and R. K. Kalia, J. Appl. Phys. **95**, 5316 (2004).
[20] S. Ogata and R. Belkada, Comput. Mater. Sci. **30**, 189 (2004).
[21] C. Muhlstein, S. Brown, and R. O. Ritchie, Sens. Actuators, A **94**, 177 (2001).
[22] F. H. Stillinger and T. A. Weber, Phys. Rev. B **31**, 5262 (1985).
[23] K. Tsuruta, C. Totsuji, H. Totsuji, and S. Ogata, Trans. Mater. Res. Soc. Jpn. **29**, 3669 (2004).
[24] M. Svensson, S. Hymbel, R. D. F. Froese, T. Matsubara, S. Sieber, and K. Morokuma, J. Comput. Chem. **100**, 19357 (1996).
[25] U. Eichler, C. M. Kölmel, and J. Sauer, J. Comput. Chem. **18**, 463 (1996).
[26] S. Dapprich, I. Komáromi, K. S. Byun, K. Morokuma, and M. J. Frisch, J. Mol. Struct.: THEOCHEM **461–462**, 1 (1999).
[27] S. Ogata (unpublished).
[28] J. P. Perdew, K. Burke, and M. Ernzerhof, Phys. Rev. Lett. **77**, 3865 (1996).
[29] A. Brandt, Math. Comput. **31**, 333 (1977).
[30] T. Ono and K. Hirose, Phys. Rev. Lett. **82**, 5016 (1999).
[31] R. S. Mulliken, J. Chem. Phys. **23**, 1833 (1955).
[32] D. Sánchez-Portal, E. Artacho, and J. M. Soler, J. Phys.: Condens. Matter **8**, 3859 (1996).
[33] W. A. Curtin and R. E. Miller, Modell. Simul. Mater. Sci. Eng. **11**, R33 (2003).
[34] F. H. Streitz and J. W. Mintmire, Phys. Rev. B **50**, 11996 (1994).
[35] D. Frenkel and B. Smit, *Understanding Molecular Simulations* (Academic, New York, 2002).
[36] K. C. Pandey, Phys. Rev. Lett. **49**, 223 (1982).
[37] R. Konecny and D. J. Doren, J. Chem. Phys. **106**, 2426 (1997).
[38] J.-H. Cho, K. S. Kim, S.-H. Lee, and M.-H. Kang, Phys. Rev. B **61**, 4503 (2000).
[39] K. Akagi and M. Tsukada, Surf. Sci. **438**, 9 (1999).
[40] Y. J. Chabal and S. B. Christman, Phys. Rev. B **29**, 6974 (1984).
[41] C. U. S. Larsson, A. L. Johnson, A. Flodström, and T. E. Madey, J. Vac. Sci. Technol. A **5**, 842 (1987).
[42] M. Chander, Y. Z. Li, J. C. Patrin, and J. H. Weaver, Phys. Rev. B **48**, 2493 (1993).
[43] L. Andersohn and U. Köhler, Surf. Sci. **284**, 77 (1993).
[44] B. B. Stefanov and K. Raghavachari, Appl. Phys. Lett. **73**, 824 (1998).
[45] M. K. Weldon, B. B. Stefanov, K. Raghavachari, and Y. J. Chabal, Phys. Rev. Lett. **79**, 2851 (1997).